NeuroImage 221 (2020) 117200

Contents lists available at ScienceDirect

NeuroImage

journal homepage: www.elsevier.com/locate/neuroimage

The **A**msterdam Ultra-**h**igh fi**e**ld **a**dult lifespan **d**atabase (AHEAD): A freely available multimodal 7 Tesla submillimeter magnetic resonance imaging database

Anneke Alkemade[a,*], Martijn J Mulder[a,c], Josephine M Groot[a], Bethany R Isaacs[a,b], Nikita van Berendonk[a], Nicky Lute[a,d], Scott JS Isherwood[a], Pierre-Louis Bazin[a,f], Birte U Forstmann[a]

[a] *Integrative Model-based Cognitive Neuroscience Research Unit, University of Amsterdam, , Nieuwe Achtergracht 129B | Room G3.08, Postbus 15926,1001 NK Amsterdam, The Netherlands*
[b] *Department of Experimental Neurosurgery, Maastricht University Medical Centre, Maastricht, The Netherlands*
[c] *Psychology and Social Sciences, University of Utrecht, Utrecht, The Netherlands*
[d] *Clinical Neuropsychology, Vrije University, Amsterdam, The Netherlands*
[f] *Max Planck Institute for Human, Cognitive and Brain Sciences, Leipzig, Germany*

ARTICLE INFO

Keywords:
Ultra-high field 7 Tesla structural MRI
Subcortex
Probabilistic maps
Basal ganglia

ABSTRACT

Normative databases allow testing of novel hypotheses without the costly collection of magnetic resonance imaging (MRI) data. Here we present the **A**msterdam Ultra-**h**igh fi**e**ld **a**dult lifespan **d**atabase (AHEAD). The AHEAD consists of 105 7 Tesla (T) whole-brain structural MRI scans tailored specifically to imaging of the human subcortex, including both male and female participants and covering the entire adult life span (18–80 yrs). We used these data to create probability maps for the subthalamic nucleus, substantia nigra, internal and external segment of the globus pallidus, and the red nucleus. Data was acquired at a submillimeter resolution using a multi-echo (ME) extension of the second gradient-echo image of the MP2RAGE sequence (MP2RAGEME) sequence, resulting in complete anatomical alignment of quantitative, R_1-maps, $R_2{}^*$-maps, T_1-maps, T_1-weighted images, $T_2{}^*$-maps, and quantitative susceptibility mapping (QSM). Quantitative MRI maps, and derived probability maps of basal ganglia structures are freely available for further analyses.

1. Introduction

Detailed imaging of the entire human brain using Magnetic Resonance Imaging (MRI) is a major challenge. In recent years, considerable efforts in the neurosciences have been dedicated to building normative databases, including the Human Connectome Project (Van Essen et al., 2012), the UK Biobank (Sudlow et al., 2015) and the Brain Genomics Superstruct Project (Holmes et al., 2015). Such efforts are ground breaking as they allow testing of novel hypotheses without the new collection of costly MRI data (Gorgolewski et al., 2016). At the same time, they help to overcome the reproducibility crisis (Open Science Collaboration, 2015).

Normative brain databases already show their value through the publication of cortical atlas maps based on multi-modal MRI data (Glasser et al., 2016). Interestingly, the neocortex which consists of six layers with varying neuronal architecture, and myelination patterns (Nieuwenhuys, 2013; Zilles and Amunts, 2010) receives most attention. This research obscures equally valuable research regarding the subcortex (Johansen-Berg, 2013). Moreover, the subcortex provides a distinct anatomical challenge with approximately 455 individual subcortical structures identified in each hemisphere, together accounting for about $\frac{1}{4}$ of the human brain volume (Alkemade et al., 2013; Forstmann et al., 2017). In addition to the anatomical characteristics, the challenges associated with MRI also differ between cortex and subcortex. Subcortical structures are often small in size, and a subset has a high iron content, which affects MRI relaxation rates. Relatedly, the iron content in individual structures is not stable over the lifespan and iron increases as a result of age-related accumulation (Aquino et al., 2009). The large physical distance of the subcortical brain structures to the MRI coils pose an additional challenge. The same holds for the prominence of pulsation artifacts. These factors together must be accommodated to obtain reliable and detailed images of the human subcortex. We found that for our subcortical atlasing efforts across the entire adult life-span, no existing database met the requirements that would allow us to answer our research questions.

Fortunately, the technical challenges are not insurmountable, and it is possible to define a specific set of requirements for MRI sequences allowing detailed imaging of both the subcortex and the cortex in a single scan. 7 Tesla is of particular interest given the high signal-to-noise ratios that can be obtained in a limited acquisition period. Pre-

* Corresponding author.
E-mail address: jmalkemade@gmail.com (A. Alkemade).

https://doi.org/10.1016/j.neuroimage.2020.117200
Received 1 July 2020; Accepted 22 July 2020
Available online 1 August 2020

Table 1
Comparison of normative 7 Tesla databases.

Database	Participants (7T)	Structural/ functional MRI	Submillimeter resolution	Image contrasts from a single scan
AHEAD	105	Structural	Yes	Yes
ATAG	53	Structural	Yes	No
Tardif et al., 2016	28	Structural	Yes	No
Hanke et al., 2014*	20	Functional	No	No
Human Connectome Project*	184	Functional	No	No

* These initiatives make use of 3T structural and 7T functional MRI data.

vious studies from our group have focused on the imaging and atlasing of the human basal ganglia, tackling the challenges, and quantifying the added value of tailored MRI approaches for small subcortical structures including the subthalamic nucleus (Alkemade et al., 2018; A. 2013; Keuken et al., 2014). Based on previous publications combined with the latest advances in 7T MRI, we have applied a submillimeter, 0.7 mm isotropic, multi-echo whole-brain 7T MRI sequence. This sequence allows detailed imaging of the whole brain including the subcortex, and the computation of quantitative contrasts from a single scan acquired with an 0.7 mm isotropic resolution, and a reconstructed $0.64 \times 0.64 \times 0.7 = 0.287$ mm^3 voxel size (Caan et al., 2019). The contrasts are collected in the **A**msterdam Ultra-**h**igh fi**e**ld **a**dult lifespan **d**atabase (AHEAD). AHEAD can be reused for studies on both the human subcortex and on the cortex. We have summarized the similarities and the differences between the AHEAD and other unrestricted available databases, to illustrate the added value of the AHEAD to the research community (Table 1). The data presented in Table 1 are limited to 7T databases, although we would like to acknowledge the importance of collections obtained at lower field strengths and collections of MRI scans in disease populations. The Brain Imaging Data Structure (BIDS) format (Gorgolewski et al., 2016) has been implemented with minor adaptations to provide a comprehensible folder structure that is easily accessible and allows for simple reuse of individual scans, as well as for algorithmic analytical approaches.

2. Participants and methods

2.1. Participants

Healthy participants were recruited via newsletters and social media of the Dutch Parkinson Foundation, as well as via the University of Amsterdam. All participants were contacted by phone to assess their suitability to participate in our study. Inclusion criteria were age 18–80y and self-reported health at the time of inclusion. Exclusion criteria were the absence of a signed informed consent, as well as any factors that could potentially interfere with MRI scanning. This included MRI incompatibility (e.g., pacemakers), pregnancy as well as self-reported claustrophobia. At least 6 male and 6 female participants were included in each age-group to ensure full coverage of the adult lifespan. The youngest age-group contains data specifically acquired for the current project, extended with data of young healthy adult participants that were scanned using the same sequence in other projects in our research group. This age-group is therefore larger. Each participant received a financial compensation of 20 Euros.

2.2. MRI scanning

Images were acquired at the Spinoza centre for Neuroimaging in Amsterdam, the Netherlands using a Philips Achieva 7T MRI scanner with a 32-channel head array coil. Routine quality checks were performed on a weekly basis at the scanner site. T1w, T2* contrasts were obtained using a MP2RAGEME (multi-echo magnetization-prepared rapid gradient echo) sequence (Caan et al., 2019). The MP2RAGEME is an extension of the MP2RAGE sequence by Marques et al. (2010) and consists of two rapid gradient echo ($GRE_{1,2}$) images that are acquired in sagittal plane after a 180° degrees inversion pulse and excitation pulses with inversion times $TI_{1,2}$ = [670 ms, 3675.4 ms]. A multi-echo readout was added to the second inversion at four echo times (TE_1= 3 ms, $TE_{2,1-4}$ = 3, 11.5, 19, 28.5 ms). Other scan parameters include flip angles $FA_{1,2}$ = [4°, 4°]; $TR_{GRE1,2}$ = [6.2 ms, 31 ms]; bandwidth = 404.9 MHz; $TR_{MP2RAGEME}$ = 6778 ms; acceleration factor $SENSE_{PA}$ = 2; FOV = 205 × 205 × 164 mm; acquired voxel-size = 0.7 × 0.7 × 0.7 mm; acquisition matrix was 292 × 290; reconstructed voxel size resulting from a built-in feature of the Philips system = 0.64 × 0.64 × 0.7 mm; turbo factor (TFE) = 150 resulting in 176 shots; Total acquisition time = 19.53 min. MRI parameters were chosen to accommodate both visualization of the cortex and subcortex, and a relatively conservative acceleration factor was chosen to ensure good image quality and acceptable noise levels. Previous reports showed limited motion artifacts, which did not result in noticeable image degradation (Caan et al., 2019). We did not perform any motion correction.

T1-maps were computed using a look-up table (Marques et al., 2010). T2*-maps were computed by least-squares fitting of the exponential signal decay over the multi-echo images of the second inversion. For QSM, phase maps were pre-processed using iHARPERELLA (integrated phase unwrapping and background phase removal using the Laplacian) of which the QSM images were computed using LSQR (Li et al., 2015; Li et al., 2014). Scans were reoriented using the fslreorient2std tool and skull information was removed through creation of a binary mask using brain extraction tool (BET) as described previously (Alkemade et al., 2017; Forstmann et al., 2014). For skull stripping we used the first echo of the second inversion. All individual MRI data were visually inspected at: 1) the time of scan acquisition, 2) during (pre)processing of the T1w, T1/R1maps, T2*/R2*maps, and quantitative susceptibility maps (QSM), and 3) when performing manual delineations.

No personal information was included in the header file. Random participant numbers were assigned to comply with general data protection regulations. Additionally, all skull information was removed, resulting in a separate image through creation of a binary mask using brain extraction protocol (BET)(Alkemade et al., 2017). Skull stripping was needed for QSM calculations, and at the same time ensured the removal of identifying facial features.

2.3. Probability atlases

Probability atlases were generated based on the manual delineations. First, group averages were obtained by co-registering first each individual R1 maps to the MNI 2009b template (Fonov et al., 2011) with the SyN algorithm in ANTs (Avants et al., 2008), using successively rigid, affine, and non-linear transformations with high levels of regularization as recommended for the subcortex (Ewert et al., 2019) and mutual information as cost function. The individual transformations were used to combine individual quantitative maps into a multimodal AHEAD template (median of R1, R2* and QSM respectively over the entire database), and the individual multimodal AHEAD maps were co-registered a second time, now to the AHEAD template, using all three quantitative contrasts. Once individual images were co-registered, the corresponding delineation masks were transformed to match the AHEAD template using linear interpolation. The transformed masks were finally

Table 2
Demographics of the healthy participants included in the **A**msterdam Ultra-**h**igh fi**e**ld **a**dult lifespan **d**atabase (AHEAD).

Age (yrs)	*Female*	*Male*	Total
18–30	27	15	42
31–40	6	6	12
41–50	6	7	13
51–60	7	5	12
61–70	7	6	13
71–80	7	6	13
total	**60**	**45**	**105**

Table 3
Overview of the file structure of AHEAD database in the Brain Imaging Data Structure format (BIDS).

/sub-0001/ses-1/anat/	
BET/	
T1w	_mod-t1w_orient-std_brain.nii.gz
T1 map	_mod-t1map_orient-std_brain.nii.gz
R1 map	_mod-r1map_orient-std_brain.nii.gz
T2* map	_mod-t2starmap_orient-std_brain.nii.gz
R2* map	_mod-r2starmap_orient-std_brain.nii.gz
QSM	_mod-qsm_orient-std_brain.nii.gz

For each subject, a subject folder (sub-0001) was created, containing a scan session folder (ses-1) with anatomical (structural) images (anat). For each of those images we collected a version that was reoriented to the standard (MNI) brain (reoriented folder). Additionally, brain extracted images (BET) were collected separately. File names include modality labels (_mod-), orientation (_orient-std) and brain extracted (_brain) labels.

averaged over the subject database, indicating for each voxel the proportion of the database inside each structure.

3. Results

3.1. Description of the database

Here, we provide a description and the results of the AHEAD, a whole-brain 7T imaging database consisting of quantitative contrasts that allow clear visualization of subcortical as well as cortical structures, and which is freely accessible for additional analyses. 106 healthy participants were scanned, 105 are included in the database. Visual inspection of all scans led us to conclude that participant motion was limited, and did not result in noticeable image degradation, apart from a single of a male aged 51–60. The scans of this participant were excluded due to low quality (Table 2).

From the MP2RAGEME scan we calculated QSM, R_1-map, $R_2{}^*$-map, T_1-map, T_1-weighted contrasts, and a $T_2{}^*$-map with a reconstructed voxel size of 0.64 × 0.64 × 0.7 mm = 0.287 mm^3. Since contrasts were derived from a single scan (see Fig. 1 for the processing pipeline), quantitative maps were fully aligned and did not require any co-registration (Fig. 2). All images were reoriented to match the radiological display convention.

Data was organized using the BIDS format, a standard for organizing and describing MRI datasets (Gorgolewski et al., 2016), with minor adaptations to accommodate our research data (see Table 3). The data structure is compatible with existing MRI toolboxes, allowing algorithmic investigations of the data.

3.2. Probabilistic atlases

To investigate the potential application of the data, we tested whether the data allowed reliable manual delineation of individual subcortical structures as described previously by our group (Alkemade et al., 2017; Keuken et al., 2013; Keuken and Forstmann, 2015). Already, we have used AHEAD to create atlases of individual basal ganglia nuclei including the subthalamic nucleus (STN), the substantia nigra (SN), the red nucleus (RN), and the internal and external segment of the globus pallidus (GPi and GPe, respectively). Manual delineations by two independent raters and Dice scores reflecting interrater reliability for the STN, SN, RN, GPi, and GPe are reported in Table 4. 3D renderings of the probability maps are shown in Fig. 3.

It is important to note that multiple raters were involved in delineating the structures, to cover the workload associated with the manual delineations (105 subjects * 5 structures * 2 hemispheres = 1050 individual masks). To this end, a group of raters were trained on two practice datasets using illustrated descriptions of example delineations to ensure a systematic approach. After familiarizing themselves with the anatomical structures, the practice datasets were parcellated according to standardized delineation protocols (Supplement 1). These initial efforts were then discussed with a trained neuroanatomist and adjusted if required. After the initial training sessions, raters performed parcellations in a randomized order, and blind to the age and sex of the individual volunteers.

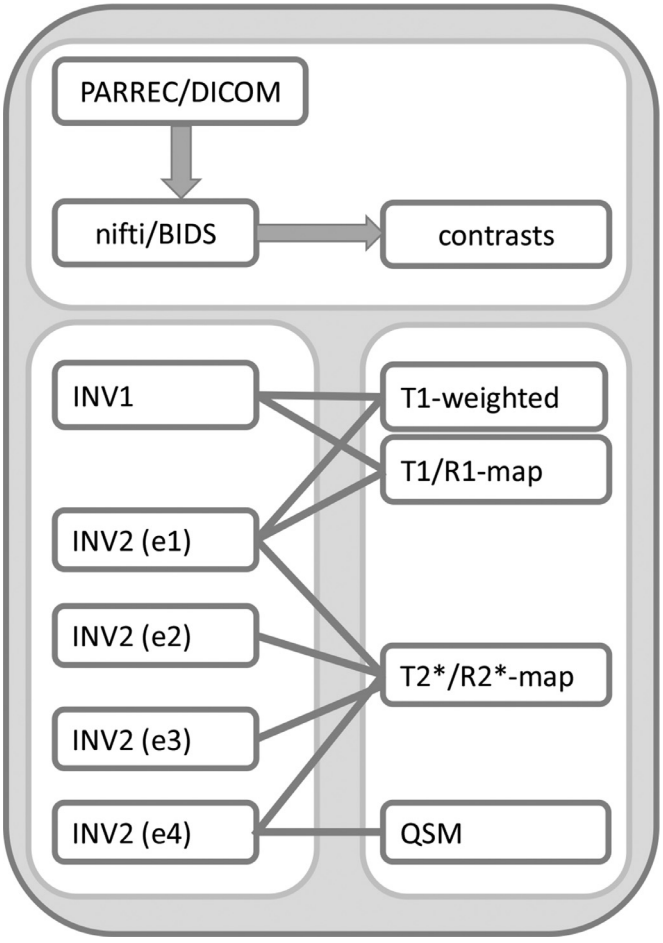

Fig. 1. Schematic overview of the quantitative maps derived from the raw Philips PAR/REC format of a multi-echo (ME) extension of the second gradient-echo image of the MP2RAGE sequence (MP2RAGEME) sequence acquisition (Caan et al., 2019). INV1 and INV2 are the gradient echo images, with the latter acquired at 4 different echo times (e1–4). Different contrast are derived and calculated for each of these gradient echo images.

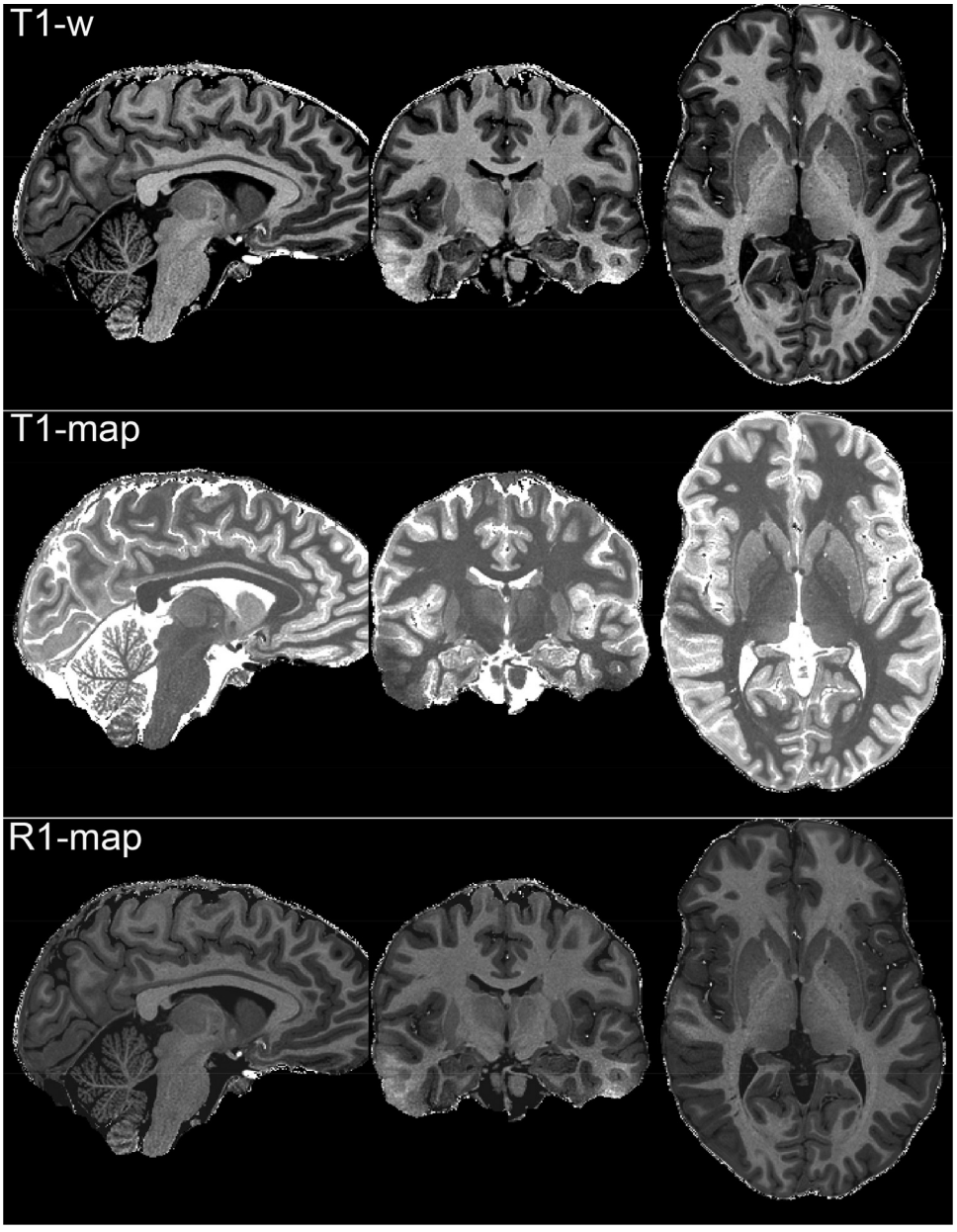

Fig. 2. Individual quantitative maps of a participant from the AHEAD database, reconstructed voxel size 0.64 x 0.64 x 0.7 mm^3.

3.3. Data sharing

The data described here, as well as the probability maps are available via Figshare (https://doi.org/10.21942/uva.10007840.v1). Per participant, we provide whole brain anatomical contrasts. The data are converted to the Nifti format, which were used for the creation for the quantitative maps included in the BET folders. Individual structure delineations were performed on these contrasts. For each individual participant, we have provided information on their age group and their sex. Characteristics of the participants are summarized in the participants.csv file, which can be used by other researchers to select participants that they would like to reuse our data.

4. Discussion

Here we provide a first release of the AHEAD, with 105 structural quantitative, submillimeter resolution 7T MRI scans across the adult lifespan. This database will be extended in the future with additional structural as well as functional MRI data. To ensure that future additions to the database are of substantial value, their description will be offered for scientific publication to ensure that they will undergo peer review providing a rigorous quality check of these future efforts. The applicability of the database is broad. Our short term goals for the database are to perform individual fingerprinting of the participants by re-inviting them to investigate brain-behavior relationships, and to map out individual structure and function. Further studies investigating brain-behavior relations have already been performed (Fontanesi et al., 2019). Midterm goals include the creation of more extensive subcortical MRI atlases across the adult life span with very high precision, and the creation of age-specific templates, as well as quantitative comparisons of MRI parameters across the adult lifespan. These will be made freely available to the field for reuse independent of the structural input of the database. Additionally, participants are currently being re-invited for a second scan session, repeating the structural MRI scan protocol, which will allow intensive studies on retest reliability. Since the initial publication of the MP2RAGEME sequence (Caan et al., 2019), a 3D Echo Planar Imaging (3D-EPI) fat-exciting motion-navigator (FatNav) was inserted into the sequence after the two GRE readout blocks allowing retrospec-

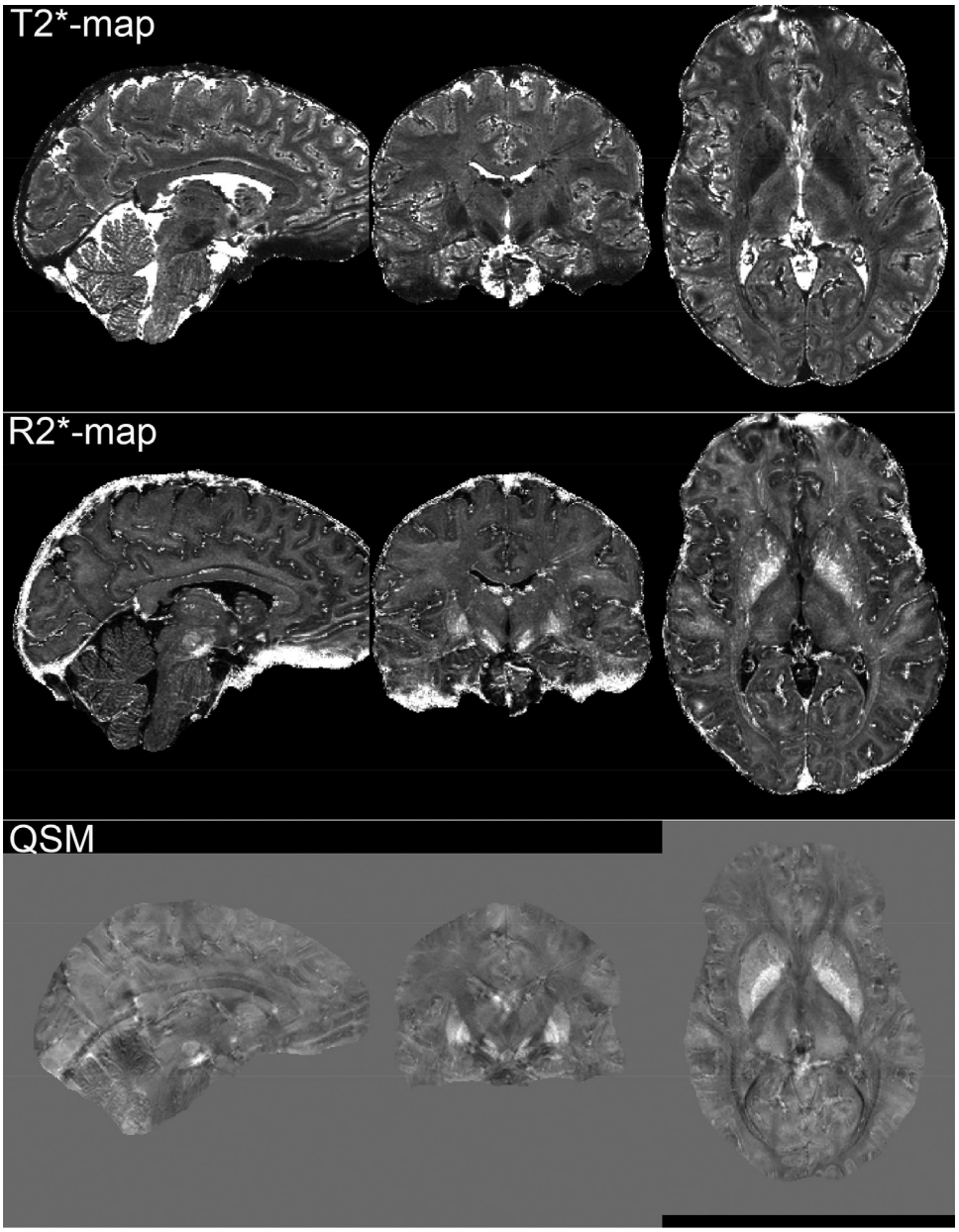

Fig. 2. Continued

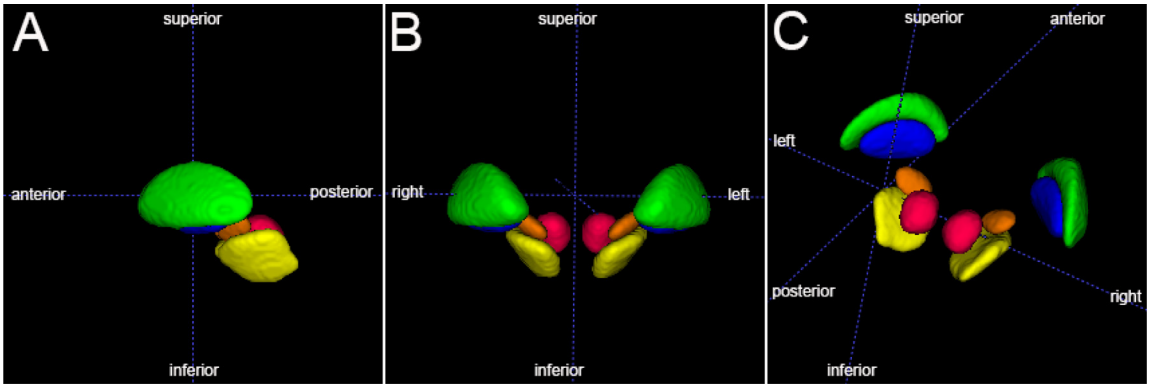

Fig. 3. 3D rendering of the average probability maps of the GPe = globus pallidus external segment (green), GPi = globus pallidus internal segment (blue), SN = substantia nigra (yellow), STN = subthalamic nucleus (orange), RN = red nucleus based (red) on the manual parcellation of 105 individual datasets.

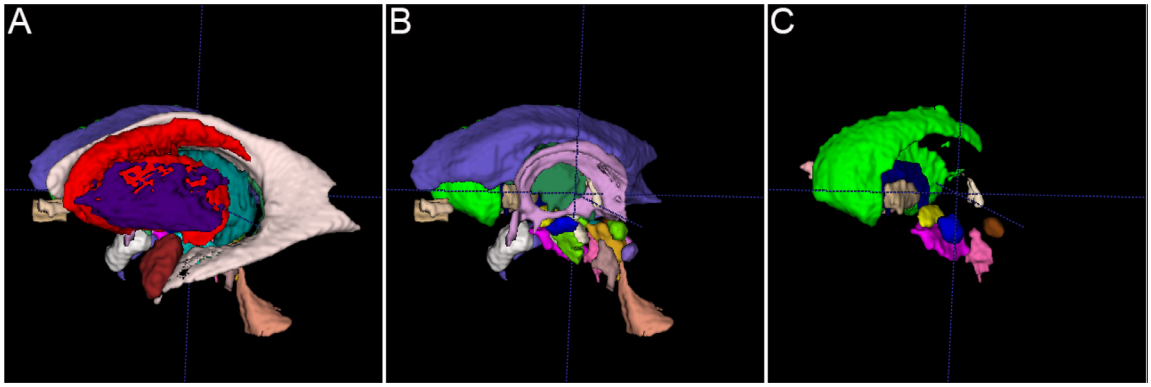

Fig. 4. Example of manual delineations of 19 individual anatomical structures in both hemispheres; A, B, and C show different views delineated on structural scans of a single subject. Included are the amygdala (A, bordeaux), claustrum (A, purple), fornix (B, lavender), internal (C, beige) and external segment (C, blue) of the globus pallidus, habenula (C, white), inferior colliculus (C, brown), internal capsule (A, dark green), pedunculopontine nucleus (C, pink), periaqueductal/periventricular gray (B, yellow ochre), red nucleus (B, blue), striatum (A, red), subcallosal cingulate gyrus (A/B, beige), subthalamic nucleus (C, yellow), substantia nigra (C, dark pink), thalamus (B, dark green), superior colliculus (B/C, light green/brown), ventral tegmental area (B, green), ventricular system (4V:A/B, beige; LV:A/B, lilac/white). See Video 1 for all structures included. Note that the structures do not appear smoothed as a result of irregularities in individually delineated structures as presented here.

Table 4.
Volumes and Dice scores for basal ganglia structures.

		Volume (mm^3)	SD	Dice	SD
STN	Left	79.74	23.46	0.74	0.10
	Right	85.18	24.66	0.75	0.10
	Average	82.46	22.56	0.75	0.09
SN	Left	461.67	91.09	0.83	0.04
	Right	478.13	94.18	0.84	0.05
	Average	469.90	88.79	0.84	0.04
RN	Left	241.12	34.60	0.91	0.03
	Right	236.49	37.91	0.90	0.06
	Average	238.80	34.16	0.91	0.04
GPe	Left	861.80	164.51	0.80	0.06
	Right	858.80	134.15	0.81	0.04
	Average	860.30	137.66	0.81	0.05
GPi	Left	360.84	88.66	0.78	0.11
	Right	355.01	88.94	0.78	0.09
	Average	358.46	80.96	0.78	0.09

GPe = globus pallidus external segment, GPi = globus pallidus internal segment, SN = substantia nigra, STN = subthalamic nucleus, RN = red nucleus. SD = standard deviation.

tive motion correction, which significantly improved image sharpness (Bazin et al., 2020). This improvement will be included in the second scan session. Long term goals include the translation and validation of our subcortical atlases for their use in clinical populations, to facilitate anatomical orientation for clinical purposes including deep brain stimulation procedures. Finally *post mortem* scans of a set of *post mortem* human brain specimens will be added, contributing even higher anatomical detail, and providing an anatomical ground truth (Alkemade et al., 2018). In addition to our own research interests, the AHEAD lends itself for the development and application of other types of analyses including machine learning approaches (Kim et al., 2019).

In our initial release here, we have included probabilistic maps of five subcortical structures providing proof of concept (Fig. 4). We have not performed any quantitative comparisons to other valuable atlases, since the results of such comparisons would be strongly influenced by the applied registration procedure selected. To be able to assess the effects of voxels shape and size on the creation of atlases for small brain structures we have previously performed simulation studies (Mulder et al., 2019). These simulation studies showed that the effects of voxel size and geometry are more pronounced in small structures, such as those of the subcortex. Additionally, we showed that voxel size should not exceed 5% of the volume of the delineated structure. These findings provide a theoretical basis for the benefit of submillimeter MRI scans for studies on the human subcortex. Another feature of the MP2RAGEME contrasts shared, is their intrinsic alignment, since they are all derived from a single scan acquisition. This allows the use of multiple contrasts for the delineation of a single structure. Additional anatomical structures will be manually delineated to create a more extensive atlas of the human subcortex. Manual outlines of a number of these structures are illustrated for a single participant in Fig. 4. We have previously calculated the time investment that is required to perform manual delineations of the ~450 individual subcortical structures is 12,000 years (Alkemade et al., 2013). This is not a realistic time investment, and therefore we have created a list of high priority structures that we intend to parcellate, and that we will include in future releases extending the database. Since the creation of these prioritized maps will also take time, and given the value of the individual probabilistic maps per structure for ongoing research, as well as the value of the reuse of the individual MRI data, we feel that sharing this resource at this stage in time would better serve the field then waiting for the completion of the atlases.

Our normative database differs from other publicly available 7T datasets, including the Human Connectome (sub) Project, the data from Hanke et al. (2014), Tardif et al., al.(2016) and the ATAG dataset (2013), in multiple ways. Most importantly: 1) the AHEAD contains *quantitative* 7T structural MRI data, 2) scans are acquired with a *submillimeter* resolution, 3) the sequence produces perfectly co-aligned MR contrasts that allow visualization of both cortical and subcortical areas (see Table 1). We have not included any quantitative comparisons to these databases, since each of these databases was created to answer different research questions. Quantitative comparisons of the suitability of these datasets to create subcortical atlases would result in a ranking of the databases that would not necessarily be useful for answering other research questions. We would therefore like to suggest that research groups interested in reusing our dataset, or any of the other available datasets define and compare their own criteria for selecting an optimal database for their studies. Compared to our previous effort with the ATAG atlas (Forstmann et al., 2014; Keuken et al., 2014; Keuken et al., 2013), the AHEAD has a finer resolution in age range, and provides anatomically perfectly matched quantitative measures of T1, T2*, and QSM which may be used to model myelin and iron concentrations in brain tissue (Stüber et al., 2014). We would like acknowledge that there is an increasing number of techniques available to calculate QSM contrasts. We decided to share the QSM contrasts that were used to create the delineations which formed the basis of the probability maps presented with

the dataset. The largest challenge with the creation of manual delineation of a larger number of individual anatomical structures is the increased workload. We are currently fine-tuning optimized methods to automatically segment larger structures (Visser et al., 2016a, 2016b). Furthermore, we hope that sharing the data as a resource will also encourage other research groups to develop and reuse (semi-)automated delineation procedures (Bazin et al., 2020, 2019; Bazin et al., 2014; Huntenburg et al., 2018). The development of such atlasing efforts will help lighten the load, and will bring us closer to a complete MRI atlas of the human subcortex.

Acknowledgments

The authors would like to thank Drs. Matthan Caan, Wietske van der Zwaag and Mr. Steven Miletic for their technical expertise, and all the undergraduate students that have contributed to the parcellations and that assisted with creating and testing of the parcellation protocols. The research described here is financially supported by STW/NWO (#14017, BUF, MJM and AA), ERC PoC (BUF), NWO Vici (BUF).

Supplementary materials

Supplementary material associated with this article can be found, in the online version, at doi:10.1016/j.neuroimage.2020.117200.

References

Alkemade, A., de Hollander, G., Keuken, M.C., Schäfer, A., Ott, D.V.M., Schwarz, J., Weise, D., Kotz, S.A., Forstmann, B.U., 2017. Comparison of T2*-weighted and QSM contrasts in Parkinson's disease to visualize the STN with MRI. PLoS ONE 12, e0176130. doi:10.1371/journal.pone.0176130.

Alkemade, A., Groot, J.M., Forstmann, B.U., 2018. Do we need a human post mortem whole-brain anatomical ground truth in in vivo magnetic resonance imaging? Front. Neuroanat 12, 110. doi:10.3389/fnana.2018.00110.

Alkemade, A., Keuken, M.C., Forstmann, B.U., 2013. A perspective on terra incognita: uncovering the neuroanatomy of the human subcortex. Front. Neuroanat. 7. doi:10.3389/fnana.2013.00040.

Aquino, D., Bizzi, A., Grisoli, M., Garavaglia, B., Bruzzone, M.G., Nardocci, N., Savoiardo, M., Chiapparini, L., 2009. Age-related Iron deposition in the basal ganglia: quantitative analysis in healthy subjects. Radiology 252, 165–172. doi:10.1148/radiol.2522081399.

Avants, B.B., Epstein, C.L., Grossman, M., Gee, J.C., 2008. Symmetric diffeomorphic image registration with cross-correlation: evaluating automated labeling of elderly and neurodegenerative brain. Med. Image Anal. 12, 26–41. doi:10.1016/j.media.2007.06.004.

Bazin, P.-L., Alkemade, A., Mulder, M.J., Henry, A.G., Forstmann, B.U., 2020. Multi-contrast Anatomical Subcortical Structures Parcellation. bioRxiv, 115865 doi:10.1101/2020.05.26.115865, 2020.05.26.

Bazin, P.-L., Alkemade, A., van der Zwaag, W., Caan, M., Mulder, M., Forstmann, B.U., 2019. Denoising high-field multi-dimensional MRI with local complex PCA. Front. Neurosci. 13, 1066. doi:10.3389/FNINS.2019.01066.

Bazin, P.L., Weiss, M., Dinse, J., Schäfer, A., Trampel, R., Turner, R., 2014. A computational framework for ultra-high resolution cortical segmentation at 7 Tesla. Neuroimage. doi:10.1016/j.neuroimage.2013.03.077.

Caan, M., Bazin, P.-L., Marques, J., de Hollander, G., Dumoulin, S., van der Zwaag, W., 2019. MP2RAGEME: T1, T2* and QSM mapping in one sequence at 7 Tesla. Hum. Brain Mapp..

Ewert, S., Horn, A., Finkel, F., Li, N., Kühn, A.A., Herrington, T.M., 2019. Optimization and comparative evaluation of nonlinear deformation algorithms for atlas-based segmentation of DBS target nuclei. Neuroimage 184, 586–598. doi:10.1016/j.neuroimage.2018.09.061.

Fonov, V., Evans, A.C., Botteron, K., Almli, C.R., McKinstry, R.C., Collins, D.L., 2011. Unbiased average age-appropriate atlases for pediatric studies. Neuroimage 54, 313–327. doi:10.1016/j.neuroimage.2010.07.033.

Fontanesi, L., Gluth, S., Rieskamp, J., Forstmann, B.U., 2019. The role of dopaminergic nuclei in predicting and experiencing gains and losses: a 7T human fMRI study. bioRxiv732560. doi:10.1101/732560.

Forstmann, B.U., de Hollander, G., van Maanen, L., Alkemade, A., Keuken, M.C., 2017. Towards a mechanistic understanding of the human subcortex. Nat. Rev. Neurosci. 18, 57–65. doi:10.1038/nrn.2016.163.

Forstmann, B.U., Keuken, M.C., Schafer, A., Bazin, P.-L., Alkemade, A., Turner, R., 2014. Multi-modal ultra-high resolution structural 7-Tesla MRI data repository. Sci. data 1, 140050. doi:10.1038/sdata.2014.50.

Glasser, M.F., Coalson, T.S., Robinson, E.C., Hacker, C.D., Harwell, J., Yacoub, E., Ugurbil, K., Andersson, J., Beckmann, C.F., Jenkinson, M., Smith, S.M., Van Essen, D.C., 2016. A multi-modal parcellation of human cerebral cortex. Nature 536, 171–178. doi:10.1038/nature18933.

Gorgolewski, K.J., Auer, T., Calhoun, V.D., Craddock, R.C., Das, S., Duff, E.P., Flandin, G., Ghosh, S.S., Glatard, T., Halchenko, Y.O., Handwerker, D.A., Hanke, M., Keator, D., Li, X., Michael, Z., Maumet, C., Nichols, B.N., Nichols, T.E., Pellman, J., Poline, J.-.B., Rokem, A., Schaefer, G., Sochat, V., Triplett, W., Turner, J.A., Varoquaux, G., Poldrack, R.A., 2016. The brain imaging data structure, a format for organizing and describing outputs of neuroimaging experiments. Sci. Data 3, 160044. doi:10.1038/sdata.2016.44.

Hanke, M., Baumgartner, F.J., Ibe, P., Kaule, F.R., Pollmann, S., Speck, O., Zinke, W., Stadler, J., 2014. A high-resolution 7-Tesla fMRI dataset from complex natural stimulation with an audio movie. Sci. Data 1, 140003. doi:10.1038/sdata.2014.3.

Holmes, A.J., Hollinshead, M.O., O'Keefe, T.M., Petrov, V.I., Fariello, G.R., Wald, L.L., Fischl, B., Rosen, B.R., Mair, R.W., Roffman, J.L., Smoller, J.W., Buckner, R.L., 2015. Brain genomics superstruct project initial data release with structural, functional, and behavioral measures. Sci. Data 2, 150031. doi:10.1038/sdata.2015.31.

Huntenburg, J.M., Steele, C.J., Bazin, P.-.L., 2018. Nighres: processing tools for high-resolution neuroimaging. Gigascience 7. doi:10.1093/gigascience/giy082.

Johansen-Berg, H., 2013. Human connectomics - what will the future demand? Neuroimage 80, 541–544. doi:10.1016/j.neuroimage.2013.05.082.

Keuken, M.C., Bazin, P.L., Crown, L., Hootsmans, J., Laufer, A., Muller-Axt, C., Sier, R., van der Putten, E.J., Schafer, A., Turner, R., Forstmann, B.U., 2014. Quantifying inter-individual anatomical variability in the subcortex using 7T structural MRI. Neuroimage 94, 40–46. doi:10.1016/j.neuroimage.2014.03.032.

Keuken, M.C., Bazin, P.L., Schafer, A., Neumann, J., Turner, R., Forstmann, B.U., 2013. Ultra-high 7T MRI of structural age-related changes of the subthalamic nucleus. J. Neurosci. 33, 4896–4900. doi:10.1523/JNEUROSCI.3241-12.2013.

Keuken, M.C., Forstmann, B.U., 2015. A probabilistic atlas of the basal ganglia using 7 T MRI. Data Br. 4, 577–582. doi:10.1016/j.dib.2015.07.028.

Kim, J., Duchin, Y., Shamir, R.R., Patriat, R., Vitek, J., Harel, N., Sapiro, G., 2019. Automatic localization of the subthalamic nucleus on patient-specific clinical MRI by incorporating 7 T MRI and machine learning: application in deep brain stimulation. Hum. Brain Mapp. 40, 679–698. doi:10.1002/hbm.24404.

Li, W., Avram, A.V., Wu, B., Xiao, X., Liu, C., 2014. Integrated Laplacian-based phase unwrapping and background phase removal for quantitative susceptibility mapping. NMR Biomed. 27, 219–227. doi:10.1002/nbm.3056.

Li, W., Wu, B., Liu, C., 2015. (ISMRM 2015) iHARPERELLA: an improved method for integrated 3D phase unwrapping and background phase removal. In: Proceedings of the 23rd Annual Meeting&Exhibition. Toronto #3313.

Marques, J.P., Kober, T., Krueger, G., van der Zwaag, W., Van de Moortele, P.F., Gruetter, R., 2010. MP2RAGE, a self bias-field corrected sequence for improved segmentation and T1-mapping at high field. Neuroimage 49, 1271–1281. doi:10.1016/j.neuroimage.2009.10.002.

Mulder, M.J., Keuken, M.C., Bazin, P.-.L., Alkemade, A., Forstmann, B.U., 2019. Size and shape matter: the impact of voxel geometry on the identification of small nuclei. PLoS ONE 14, e0215382. doi:10.1371/journal.pone.0215382.

Nieuwenhuys, R., 2013. The myeloarchitectonic studies on the human cerebral cortex of the vogt-vogt school, and their significance for the interpretation of functional neuroimaging data. In: Microstructural Parcellation of the Human Cerebral Cortex. Springer, Berlin Heidelberg, Berlin, Heidelberg, pp. 55–125. doi:10.1007/978-3-642-37824-9_3.

Open Science Collaboration, O.S., 2015. PSYCHOLOGY. Estimating the reproducibility of psychological science. Science 349, aac4716. doi:10.1126/science.aac4716.

Stüber, C., Morawski, M., Schäfer, A., Labadie, C., Wähnert, M., Leuze, C., Streicher, M., Barapatre, N., Reimann, K., Geyer, S., Spemann, D., Turner, R., 2014. Myelin and iron concentration in the human brain: a quantitative study of MRI contrast. Neuroimage 93, 95–106. doi:10.1016/j.neuroimage.2014.02.026.

Sudlow, C., Gallacher, J., Allen, N., Beral, V., Burton, P., Danesh, J., Downey, P., Elliott, P., Green, J., Landray, M., Liu, B., Matthews, P., Ong, G., Pell, J., Silman, A., Young, A., Sprosen, T., Peakman, T., Collins, R., 2015. UK biobank: an open access resource for identifying the causes of a wide range of complex diseases of middle and old age. PLoS Med. 12. doi:10.1371/journal.pmed.1001779.

Tardif, C.L., Schäfer, A., Trampel, R., Villringer, A., Turner, R., Bazin, P.-L., 2016. Open Science CBS Neuroimaging Repository: sharing ultra-high-field MR images of the brain. Neuroimage 124, 1143–1148. doi:10.1016/J.NEUROIMAGE.2015.08.042.

Van Essen, D.C., Ugurbil, K., Auerbach, E., Barch, D., Behrens, T.E.J., Bucholz, R., Chang, A., Chen, L., Corbetta, M., Curtiss, S.W., Della Penna, S., Feinberg, D., Glasser, M.F., Harel, N., Heath, A.C., Larson-Prior, L., Marcus, D., Michalareas, G., Moeller, S., Oostenveld, R., Petersen, S.E., Prior, F., Schlaggar, B.L., Smith, S.M., Snyder, A.Z., Xu, J., Yacoub, E., 2012. The Human Connectome Project: a data acquisition perspective. Neuroimage 62, 2222–2231. doi:10.1016/j.neuroimage.2012.02.018.

Visser, E., Keuken, M.C., Douaud, G., Gaura, V., Bachoud-Levi, A.-C., Remy, P., Forstmann, B.U., Jenkinson, M., 2016a. Automatic segmentation of the striatum and globus pallidus using MIST: multimodal Image Segmentation Tool. Neuroimage 125, 479–497. doi:10.1016/j.neuroimage.2015.10.013.

Visser, E., Keuken, M.C., Forstmann, B.U., Jenkinson, M., 2016b. Automated segmentation of the substantia nigra, subthalamic nucleus and red nucleus in 7T data at young and old age. Neuroimage 139, 324–336. doi:10.1016/j.neuroimage.2016.06.039.

Zilles, K., Amunts, K., 2010. Centenary of Brodmann's map — Conception and fate. Nat. Rev. Neurosci. 11, 139–145. doi:10.1038/nrn2776.